Eur Biophys J (2004) 33: 596–610
DOI 10.1007/s00249-004-0407-2

ARTICLE

Bryan M. van der Ende · Frances J. Sharom
James H. Davis

The transmembrane domain of Neu in a lipid bilayer: molecular dynamics simulations

Received: 17 November 2003 / Revised: 2 April 2004 / Accepted: 5 April 2004 / Published online: 9 June 2004

Abstract The results of full-atom molecular dynamics simulations of the transmembrane domains (TMDs) of both native, and Glu^{664}-mutant (either protonated or unprotonated) Neu in an explicit fully hydrated dimyristoylphosphatidylcholine (DMPC) lipid bilayer are presented. For the native TMD peptide, a 10.05 ns trajectory was collected, while for the mutant TMD peptides 5.05 ns trajectories were collected for each. The peptides in all three simulations display stable predominantly α-helical hydrogen bonding throughout the trajectories. The only significant exception occurs near the C-terminal end of the native and unprotonated mutant TMDs just outside the level of the lipid headgroups, where π-helical hydrogen bonding develops, introducing a kink in the backbone structure. However, there is no indication of the formation of a π bulge within the hydrophobic region of either native or mutant peptides. Over the course of the simulation of the mutant peptide, it is found that a significant number of water molecules penetrate the hydrophobic region of the surrounding lipid molecules, effectively hydrating Glu^{664}. If the energy cost of such water penetration is significant enough, this may be a factor in the enhanced dimerization affinity of Glu^{664}-mutant Neu.

Keywords Molecular dynamics simulation · Neu transmembrane domain · Membrane protein structure and dynamics

B. M. van der Ende · J. H. Davis (✉)
Department of Physics, University of Guelph, Guelph, Ontario, N1G 2W1, Canada
E-mail: jhd@physics.uoguelph.ca

F. J. Sharom
Chemistry and Biochemistry, University of Guelph, Guelph, Ontario, Canada

Introduction

The plasma membrane of the cell plays a central role in the regulation of cell proliferation via signal transduction through cell-surface growth factor receptors. Binding of a growth factor to members of the epidermal growth factor receptor (EGFr) family leads to dimerization of the receptor within the membrane, which in turn results in transmission of a signal for cell division to the interior of the cell. Signal transduction takes place by activation of the tyrosine kinase catalytic domain located within the cytoplasmic region of the receptor. There is currently limited structural information available for proteins in this family, although a crystal structure of the extracellular domain of human ErbB-2 (Her2) has been recently published (Cho, et al. 2003). However, it is known that the specific amino acid sequence of the transmembrane domain (TMD) is important for their function (Sternberg and Gullick 1990; Cao et al. 1992a, 1992b). The rat Neu gene encodes a 185-kDa integral membrane protein in the EGFr family, comprising a large Cys-rich extracellular domain, a TMD made up of one membrane-spanning segment, and an intracellular tyrosine kinase catalytic domain (Bargmann et al. 1986b).

A single mutation within the Neu TMD ($Val^{664} \rightarrow$ Glu/Gln) results in a protein that is oncogenic, with the ability to transform mammalian cells, causing cancer-like growth (Bargmann et al. 1986a). The mutant Neu protein has increased signalling activity as a result of greatly enhanced dimerization (Bargmann and Weinberg 1988; Weiner et al. 1989). While side-to-side dimerization of the membrane-spanning helices of such receptors appears to be key to normal signal transduction, aberrant helix–helix association can cause human disease. The human version of Neu, ErbB2 or HER2, is frequently activated in breast cancers (Hynes and Stern 1994), where its presence is predictive of poor prognosis and lower survival (Press et al, 1997), and it is currently the target of new anti-cancer therapies. Aberrant helix–

helix association with other integral proteins is also known to be the driving force in oncogenic transformation by the bovine papilloma virus E5 protein (Goldstein et al. 1992). A report by Zhou et al. (2001) indicates that several polar residues (including Glu, Gln, Asp, Asn and His), when present within hydrophobic helices, can drive helix–helix association by acting as both H-bond donors and acceptors.

The structural basis for enhanced dimerization of the mutant Neu/ErbB2 protein has been the subject of much speculation, and different models have been proposed (Brennan et al. 2000). One working hypothesis is that activating mutations stabilize the Neu dimer by promoting closer packing of the transmembrane helices, mediated by symmetric H-bonding interactions between the protonated carboxyl side-chains of Glu^{664} in the mutant Neu protein (Garnier et al. 1997). Another model proposes that a pentapeptide motif (Ala^{661}–Gly^{665}) promotes dimerization via interhelical H bonds from the carboxyl atoms of Glu^{664} to the backbone peptide carbonyl of Ala^{661} (Sternberg and Gullick 1990). Close helix packing was suggested to be essential for dimerization, and specific side-chain properties were required at three of the five positions in the motif. Earlier work of Smith et al. (1996) supported either of these models with nuclear magnetic resonance (NMR) and polarized Fourier transform infrared spectroscopy (FTIR) studies of the mutant Neu peptide, which seemed to show that Glu^{664} is in fact protonated and strongly H-bonded. More recent work by some of the same investigators, however, have demonstrated that Gln^{664} mutation sites do not so strongly couple with each other in the dimer structure (Smith et al. 2002). They further demonstrate that Gly^{665} packs into the dimer interface and interacts with Glu^{664}. Their model, arrived at using established computational search techniques that employed their measurements as constraints, also incorporates Gln^{664} interacting with the backbone of Ala^{661} and the side chain of Thr^{662}.

A more recent study by Fleishman et al. (2003), using computational exploration of conformational space, claims to have found two stable conformations of the TMD of ErbB2 which they claim correspond to the active and inactive states of the protein and that the molecule can switch between the two conformations without crossing exceedingly unfavorable states. They demonstrate in their paper how this switch mechanism provides explanations for the biochemical and oncogenic properties of ErbB2. They propose that their molecular switch model can provide explanations for the behaviour of naturally occurring variants of ErbB2, such as Neu. Molecular dynamics (MD) simulations have been used to argue that enhanced dimerization results from a conformational change in the secondary structure of the ErbB2 TMD, such that a sharp kink occurs at the site of mutation at position 664 (Brandt-Rauf et al. 1995). However, others predicted an α-helix $\rightarrow$ π-bulge transition one helical turn away from residue 664 (Duneau et al. 1996, 1997). More recent simulations explored the nature of the dimer interface of the Neu TMD, and suggested that the two helices interact preferentially to form a left-handed coiled coil (Garnier et al. 1997, 2003). Local π defects facilitating inter-helix hydrogen bond interactions were predicted to result in a change in the helix packing, leading to a symmetric dimer interface which included the site of mutation. The Glu side-chain was found to interact directly with the partner helix, either via the corresponding Glu carboxyl, or with main chain carbonyl groups. However, an early NMR study indicated that wild-type and mutant Neu peptides were α-helical in aqueous solution, in both the presence and absence of lipids, and did not show conformational differences (Gullick et al. 1992). More recently, NMR work of Smith et al. (2002) has demonstrated that Neu is α-helical in the region of the mutation site. Other groups have carried out ^{1}H-NMR experiments on 35- and 36-residue wild-type and mutant Neu TMDs in the solvent trifluoroethanol (TFE), where the peptides remained monomeric (Goetz et al. 2001; Houliston et al. 2003) and in detergent micelles (Houliston et al. 2004). The results of Goetz et al. (2001, deposited as a pdb file in the Protein Data Bank, access code 1IIJ) suggested the existence of a transition between an α-helical conformation and a π bulge, which spanned two helical turns starting six residues downstream of the site of mutation, but those of Houliston et al. (2003, 2004) showed no such tendency. More detailed information on the structure of the TMDs of this family of receptors may lead to a better understanding of the role they play in signalling processes, both normal and aberrant.

While MD simulations and molecular modelling studies themselves cannot determine protein molecular structure, they provide a powerful means of following the structural changes that occur over time. In the present work, MD simulations are carried out on 36-residue TMDs of both native and mutant Neu (both in the protonated and unprotonated form), in an explicit fully hydrated phospholipid bilayer of dimyristoylphosphatidylcholine (DMPC).

Model and methods

Construction of the initial configurations

Three separate simulations of Neu transmembrane domains (TMDs) have been performed: one native, one mutant with Glu protonated, one mutant with Glu left unprotonated. In each case, 36 amino-acid residues were included, with appropriate terminations: NTER-Gln-Arg-Ala-Ser-Pro-Val-Thr-Phe-Ile-Ile-Ala-Thr-Val-Val (or Glu or GluP)-Gly-Val-Leu-Leu-Phe-Leu-Ile-Leu-Val-Val-Val-Val-Gly-Ile-Leu-Ile-Lys-Arg-Arg-Arg-Gln-Lys-AMIDE. NTER is NH_3^+, AMIDE is an amide group, and GluP is the protonated form of Glu. In each system, the TMD is surrounded by a bilayer of 32 DMPC lipid molecules (16 to each leaflet), and over

1,480 water molecules. All setup computations were performed using version 26b1 of CHARMM (Brooks et al. 1983), and the PARAM 22 (Mackerell et al. 1992) force field that accompanies it.

The method of system construction follows a protocol pioneered by Roux and Woolf (1996). The core idea of this protocol is to assemble the membrane system using pre-equilibrated components, so that the starting configuration is as close to equilibrium as possible, thus shortening the length of the equilibration period that is needed before collecting trajectory data.

Construction

Each Neu TMD was initially constructed as an ideal right-handed α-helix ($\phi = -57.0°$, $\psi = -47.0°$). Membrane-spanning domains of proteins are typically of that conformation, and Smith et al. (1996, 2002) demonstrated with polarized FTIR and NMR that both mutant and native versions of the Neu TMD are largely α-helical, particularly in the vicinity of the key mutation point at position 664. We have adopted a canonical α-helical structure as the initial secondary structure for each TMD in our simulations, so that we could see what deformations in structure would occur with each TMD in the time span of nanoseconds. The first two dihedral angles of the amino acid side chains were initially harmonically constrained (with a force constant of 50.0 kcal/(mol Å^2)) to be at the midpoint of their optimal ranges, determined from the side-chain rotamer library of Dunbrack and Karplus (1993). Backbone atoms and the first two side-chain carbon atoms (Cβ and Cγ) were at first fixed while energy-minimizing the TMD structure, but later, harmonically constrained with the force strength iteratively decreased from 5.0 kcal/mol to zero. The side-chain dihedral angle constraints were eliminated after reducing the backbone harmonic constraints from 5.0 kcal/mol. Each TMD was rotated to align the helix axis parallel to the z axis. Further, to ensure that the hydrophobic residues would best match the lipid hydrocarbon chains in their placement in the z direction (centered at $z = 0$), the helix was positioned initially so that the backbone carbonyl carbon of Val^{666} was at $z = 0$.

Membrane construction

A unit cell with square dimensions in the x and y directions was implemented. The mean cross-section of the TMD was calculated to be 143 Å^2. Including 32 DMPC lipids (16 per leaflet) together with the TMD polypeptide in a 34×34 Å square region allowed 63.3 Å^2 per lipid. This area per lipid agrees with recent experimental work on liquid-crystalline DMPC. X-ray techniques have yielded areas of 59.5 ± 0.2 Å^2 (Koenig et al. 1997) and 59.7 ± 0.2 Å^2 (Petrache et al. 1998) at $T = 30$ °C. Deuterium NMR has been used to determine an area of 60.0 Å^2 at $T = 30$ °C and of 65.4 Å^2 at $T = 50$ °C (Petrache et al. 2000). Our simulations produced trajectories at $T = 40$ °C.

Incorporation of the DMPC lipids into the simulation systems began by finding preferred coarse-grained locations for the lipids. This search was performed by placing van der Waals spheres in the system, one for each lipid, each with a cross-sectional area equal to one lipid. The centers of the spheres were constrained to the planes $z = \pm 17$ Å (16 to one plane, the rest to the other). The TMD was placed at the center of the box and was fixed in place. The box was initially made three times larger than required, in the x and y directions, and then iteratively shrunk by 1 Å per iteration to the required dimensions. The spheres, free to move in their planes, were energy-minimized at each iteration.

DMPC lipids were randomly chosen from a library of 2,000 conformations (De Loof et al. 1991; Pastor et al. 1991; Venable et al. 1993; Hardy and Pastor 1994). The chosen lipids replaced the van der Waals spheres, which were subsequently deleted. At this point, the number of non-hydrogen atoms in bad contact with one another (within 2.6 Å of each other) was reduced by systematically rotating each lipid (picking them in random order), with its associated water molecules, about its z-axis, and subsequently translating them along grid points in the x,y plane. The entire configuration was then further energy minimized.

The entire procedure of randomly picking lipid conformations, systematically rotating and translating the lipids, and minimizing the lipids as a whole was performed for ten different sets of selected lipids (each corresponding to a different seed number). The set with the least final number of bad contacts and with lipid chains that best filled the hydrocarbon space between lipid head groups was chosen for further computation.

Water overlay

The TIP3P water model (Jorgensen et al. 1983) was employed for water molecules overlaying the TMD/lipid system. A pre-equilibrated cube (15.5516 Å^3) of 125 of these water molecules at bulk density (0.0332 Å^{-3}) was repeated throughout the x,y plane so that it filled the 34×34 Å^2 cell space (waters outside of this space were removed). This, in turn, was repeated in the z-dimension, to a height of 62.2064 Å. Using periodic images in all directions, the 34×34×62.2064 Å^3 rectangular box was energy-minimized. This equilibrated rectangular box of water molecules was then overlaid upon the lipids and the protein. In doing so, waters within 12 Å of $z = 0$ or within 2.6 Å of non-hydrogen atoms were removed, and the size of the of the unit cell in the z direction was adjusted to 74.2 Å, to give the desired level of hydration.

Each system as a whole was energy-minimized. A number of constraints were put in place for this process. A planar potential (of strength 10.0 kcal/(mol Å^2)) was placed on water molecules at $z = \pm 11$ Å to prevent penetration of water into the membrane core, and an-

other such potential (of strength 50.0 kcal/(mol Å^2)) was placed on the glycerol C2 atom of each lipid at $z = \pm 14$ Å to maintain a bilayer configuration. The protein TMD was fixed, and SHAKE (Ryckaert et al. 1977) was applied to fix all hydrogen atom bond distances.

No counterions have been included in this simulation. This does leave a net charge in each system, as the net charge of the native and protonated mutant TMDs is each +7, and the net charge of the unprotonated mutant TMD is +6. This would present a methodological issue had we been using the Particle Mesh Ewald (PME) summation technique to calculate the Coulombic forces (an approach becoming increasingly common in lipid bilayer MD simulations (Patra et al. 2003) since PME requires zero net charge in the unit cell to guarantee convergence (Darden et al. 1993). There is no such issue here, however, since we employed cutoffs with force switching during equilibration and dynamics production, using cutoff distances short enough that the TMD in the unit cell does not interact with its images.

Equilibration

To equilibrate each system, a total of 205 ps of dynamics trajectory was calculated for each system. During this time, constraints placed on each system were gradually released to ensure a smooth equilibration of each system. Integration was performed using the Verlet leap-frog algorithm (Verlet 1967), and using SHAKE to constrain hydrogen bond lengths allowed time steps of 2 fs in length to be employed. Constant-volume periodic boundary conditions were used during equilibration to allow the system to properly fill its space. Although the objective was to use constant pressure conditions for trajectory production, constant volume conditions were needed throughout the length of equilibration to avoid unwanted strains on the membrane system. Nosé-Hoover temperature control (Nosé 1984a, 1984b) was employed to regulate the temperature at 313 K (40 °C), well above the gel–liquid crystalline transition temperature of DMPC (Gennis 1989). The coupling parameter Q for this temperature control scheme was set to 3,000 kcal·ps^2. Initial atom velocities were assigned using a Gaussian Maxwell-type distribution. Electrostatic and van der Waals interaction switching began at a distance of 8 Å, and was cut off at 11 Å; the non-bonded list cut was set at 12 Å.

Dynamics production

Constant average normal pressure (in the z direction) and fixed area (in the x and y directions) were maintained using the CPT dynamics facility of CHARMM, employing the Langevin piston method (Feller et al. 1995). The collision frequency γ was set to 5.0 ps^{-1}, the piston mass W was set to 750 amu, and the reference pressure was set to 1 atm. Nosé-Hoover temperature control was employed to keep the system temperature at 313 K, as in the equilibration stage of these simulations. Non-bonded interaction cutoff was also employed in the same manner as in the equilibration stage. Leap-frog Verlet integration was performed using 1 fs time steps in the absence of applying SHAKE constraints.

Two constraints were maintained throughout dynamics production: a planar potential on the z coordinate of the collective center of mass of all of the lipids [5.0 kcal/(mol Å^2)] to prevent global drift of the bilayer, and a cylindrical potential on the protein's center of mass to prevent the TMD drifting from the origin in the x,y plane [5.0 kcal/(mol Å^2)]. The latter restraint may not have been necessary as it is generally preferable to a have a minimum number of restraints in place during dynamics production. However, Garnier et al. (2003) found it necessary to include a similar restraint to one of their helices in a simulation of oncogenic ErbB2 dimer in a DMPC bilayer. The former constraint was also employed by them, as well as by Bernèche and Roux (2000) in simulations of the KcsA K^+ channel.

At every 100 fs, coordinates were saved to binary trajectory files, and energy components were written out. Formatted coordinate files and binary restart files were written out every 5 ps. The entire trajectory length of the native simulation was 10,050 ps, and the mutant simulations each computed 5,050 ps of trajectory. These computations were performed on two Silicon Graphics Origin 200 machines employing 4 R10000 processors each. The native simulation used four processors in parallel on one machine, and the mutant simulations each used two processors on the other: 5.5 months were necessary to complete these simulations.

Analysis

Determination of the TMD helix axis

Let I_{xx}, I_{yy}, I_{zz} be principal moments of the moment of inertia tensor,

$$I_{ij} = \sum_{k=1}^{N} m_k \left[\delta_{ij} r_k^2 - r_{k_i} r_{k_j} \right]. \quad (1)$$

where N is the number of atoms, m_k is the mass of the kth atom, $\boldsymbol{r}_k$ is the position vector of the kth atom, and $i,j = \mathrm{x,y,z}$. For the Neu TMDs, the sum is restricted to backbone atoms only. Diagonalizing this tensor gives I_{xx}, I_{yy}, and I_{zz}, and their associated principal axes. This calculation is performed using atomic coordinates from coordinate files sampling the trajectory every 5 ps. As each TMD is helical in shape, I_{zz} (associated with the principal axis closely proximate to the helix axis) is the smallest principal moment. The other two moments are nearly equal to each other, reflecting the cylindrical symmetry of the peptide about the helix axis. By convention, I_{xx} is always chosen to be the larger of the two.

Radial distribution function

Solvation at Glu^{664} in the mutant TMDs was investigated through use of a radial distribution function,

$$g_{ij}(r_{ij}) = \frac{\Delta N(r_{ij})}{\rho_i \Delta V(r_{ij})} \quad (2)$$

where

$$\Delta V(r_{ij}) = \frac{4\pi}{3}\left((r_{ij} + \Delta r_{ij})^3 - r_{ij}^3\right), \quad (3)$$

is the volume of a spherical shell of thickness Δr_{ij}, $\Delta N(r_{ij})$ is the number of water molecules i in that spherical shell, r_{ij} is the radial distance from atom j, and ρ_i is the bulk number density of water molecules i. The radial distribution function is the ratio of a local density ρ_i (r_{ij}) of the atoms of type i (here, water molecules) around a specified atom j (here, the carboxyl oxygen of Glu^{664}) to the bulk density ρ_i (Haile, 1992). This function gives the likelihood of finding an atom of type i around an atom of type j as a function of radial distance r_{ij} in the local density, relative to finding the same in the bulk density.

Results and discussion

Energy components of each system

The total energy of each of the simulated systems was conserved to within 5% after the first ~200 ps of dynamics production. A short-lived initial relaxation to lower energies evident in the potential and total energies likely reflects the establishment of new equilibrium conditions due to changing the boundary conditions from constant volume (during equilibration) to constant normal pressure and constant area at the start of dynamics production. Because each of the Neu systems has essentially the same number of atoms set up in a nearly identical way, the average value of each of the energy components was essentially the same for each system. Temperature fluctuations, averaged every 5 ps, were within 1 K of the average value of 313 K.

Average density profiles of each system

Density profiles of the main system components along the bilayer normal of each system are shown in Fig. 1. These profiles are averages of separate profiles computed over mutually exclusive 300-ps-long segments of trajectory (beginning after 150 ps of dynamics). The error bars reflect the standard deviations of these 300 ps averages, indicating that all system components are quite stable throughout the course of the simulations. Details of the z distribution of the Neu TMDs, of the phosphate, choline and carbonyl groups in the lipid headgroups, of the lipid chains and of the waters are shown in these figures, and they follow patterns seen in previously published density profiles (e.g., Egberts et al. 1994; Bernèche et al. 1998). The protein component spans from about −30 Å (N-terminal end) to about 30 Å (C-terminal end), with greater density towards the C-terminal end. The center of the region of hydrophobic groups of the protein is matched with the center of the region of hydrophobic lipid chains, leaving the charged or polar groups at either end of the peptide in the region

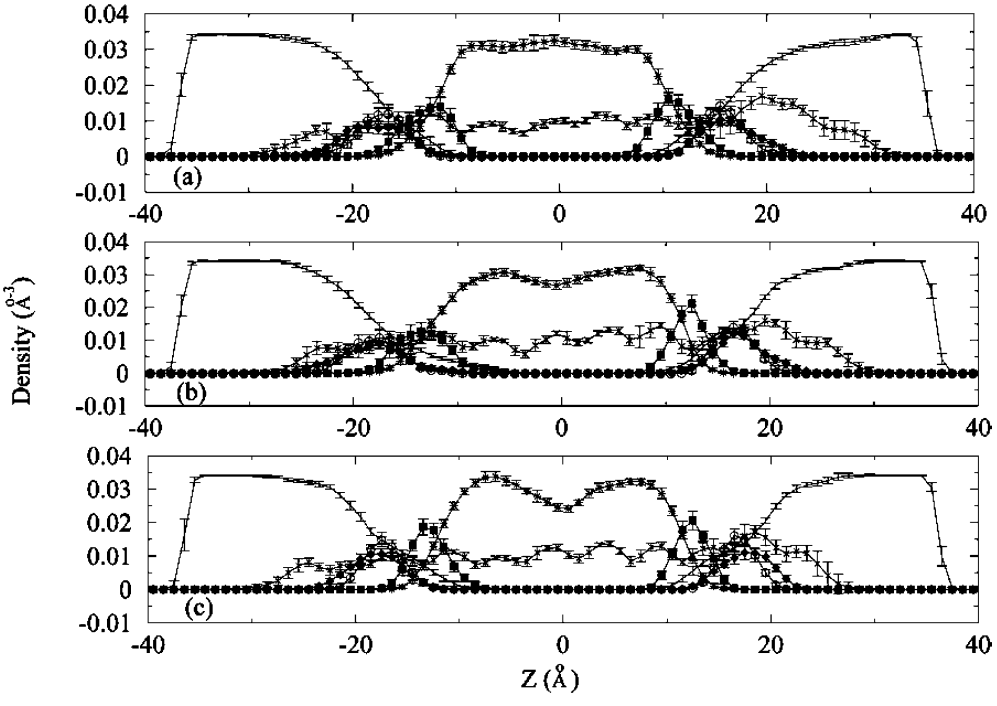

Fig. 1 The density profile of water (no symbol), peptide (×), hydrocarbon chains (*), trimethylamine groups (*filled diamonds*), phosphodiester groups (*open circles*), and ester groups (*filled squares*) along the bilayer normal for **a** the native, **b** the charged mutant, and **c** the protonated mutant TMD systems. The centre of the bilayer is at z = 0 Å. The N terminus of each TMD is below z = 0 and the C terminus of each TMD is above z = 0. Units were chosen so that the graph for water gives (molecules/Å^3)

of the lipid headgroups and the water molecules. The N-terminal end has three fewer charged/polar residues than the C-terminal end (Gln-Arg-Ala vs. Lys-Arg-Arg-Arg-Gln-Lys), explaining the greater density at the C-terminal end. Phosphate and choline groups occupy essentially the same region in both leaflets of the bilayer, showing that the average orientation of the dipole formed by these groups is nearly parallel to the bilayer surface. The distribution of the lipid headgroups spans nearly 20 Å in each leaflet. The atom distribution of the lipid chains each (except for the native system) displays a density minimum at the center of the bilayer in all but one of the systems, consistent with X-ray profiles of membranes (Franks 1976; Nelander and Blaurock 1978; Finean et al. 1984). The minimum reflects a reduction of electron density at the bilayer center, where the hydrocarbon region is most fluid. Curiously, the native Neu system (Fig. 1a) shows a small maximum in lipid chain density at the center of the bilayer. It is notable that the overall distribution of lipid chain density in that system is correspondingly narrower in the z dimension by about ~2–3 Å compared to the lipid chain density distribution in the other systems.

As Egberts et al. (1994) noted in their simulation of hydrated DPPC, lipid chain and water distributions overlap significantly with the distributions of the headgroup region, and even with each other. What is particularly interesting to note is that water densities invade the hydrophobic lipid chain/protein region much more strongly at the N-terminal end (up to about $z = -5$ Å) in the charged mutant system (Fig. 1b), than in all the other systems. This is explained by the presence of the charged Glu residue at this end of the protein, which would tend to draw polar water molecules to itself. In the native TMD, Glu is replaced by Val, which is uncharged, and the water penetration is correspondingly reduced (to $z = -9$ Å). When Glu is protonated, it is not nearly as able to draw in water molecules, and this is reflected by the fact that the water/hydrophobic region overlap of densities for the protonated mutant system is not much different from that for the native system, although both mutant peptides rest lower in the bilayer than the native peptide, with the mutation position lying close to the water interface (see below).

Peptide backbone structure

The average backbone structure of each Neu TMD is summarized in Table 1, which lists the backbone dihedral angles (ϕ, ψ, ω) and the covalent bond angles averaged over all residues in the TMD, and their standard deviations. The dihedral angle ω is reported as its deviation from 180°, and ψ has been averaged with and without the first residue at the N-terminal end, as the dihedral angle at that location is far from the mean of the rest of the residues. The ideal dihedral angles reported are those for an ideal α helix in vacuum. In comparing different systems, the mean values of the dihedral angles agree with each other within their standard deviations. They also agree with the ideal values, within their standard deviations. For comparison, Belohorcová et al. (1997) obtained very comparable average values of $\phi = -43°$ and $\psi = -64°$ in the hydrophobic region of their peptide. Bond angles from Creighton (1984)—averages from X-ray structures —are also presented for comparison. Bond angles from Engh and Huber (1991) are very similar to values cited by Creighton (1984), which also provides values for C_i-$C_{\alpha i}$-$C_{\beta i}$, N_i-$C_{\alpha i}$-C_i, and N_i-$C_{\alpha i}$-$C_{\beta i}$ that are in very good agreement with the average values obtained from the simulations.

It is striking how closely the mean dihedral and bond angles are replicated by each of the simulation systems. This is interesting in the light of the fact that it has been observed that structures derived from computational refinement of solution NMR and medium resolution X-ray structures tend to display narrower distributions of

Table 1 Time-averaged and rms peptide backbone **A** dihedral and **B** bond angles (in degrees), averaged over all applicable residues

	Native	Charged	Protonated	Ideal
(a)				
ϕ	−66.2 ± 10.7	−66.4 ± 10.7	−65.6 ± 10.1	−57
ψ	−44.9 ± 11.8	−39.8 ± 12.4	−37.3 ± 10.7	−47
Ψ (without res. 1)	−41.5 ± 9.9	−45.8 ± 11.7	−43.1 ± 9.9	−47
$\Delta\omega$	−3.94 ± 6.98	−3.18 ± 6.98	−3.39 ± 6.86	0
(b)				
	Native	Charged	Protonated	Creighton
$C_i - C_i^\alpha - C_i^\beta$	110.6 ± 3.5	110.4 ± 3.5	110.5 ± 3.5	–
$C_i - C_i^\alpha - H_i^\beta$	106.1 ± 4.3	106.2 ± 4.3	106.2 ± 4.3	–
$C_{i-1} - N_i - C_i^\alpha$	124.0 ± 3.0	124.0 ± 3.5	124.0 ± 3.5	121.9
$C_{i-1} - N_i - H$	119.2 ± 4.1	119.4 ± 4.1	119.2 ± 4.1	119.5
$C_i^\alpha - C_i - N_{i+1}$	118.5 ± 3.0	118.4 ± 3.0	118.4 ± 3.0	115.6
$C_i^\alpha - C_i - O_i$	120.7 ± 3.0	120.7 ± 3.0	120.7 ± 3.0	121.1
$C_i^\alpha - N_i - H_i$	116.1 ± 4.1	116.1 ± 4.1	116.1 ± 4.1	118.2
$C_i^\beta - C_i^\alpha - H_i^\alpha$	108.0 ± 4.1	108.1 ± 4.7	108.1 ± 4.7	–
$N_i - C_i^\alpha - C_i$	113.1 ± 3.0	112.9 ± 3.6	113.0 ± 3.6	–
$N_i - C_i^\alpha - C_i^\beta$	111.0 ± 3.5	111.0 ± 3.5	111.0 ± 3.5	–
$N_i - C_i^\alpha - H_i^\alpha$	107.6 ± 3.5	107.7 ± 3.5	107.6 ± 3.5	–
$O_i - C_i - N_{i+1}$	120.6 ± 3.0	120.7 ± 3.0	120.8 ± 3.0	123.2

angles such as $\Delta\omega$ than do high resolution X-ray structures that were not computationally refined (Davis and Auger 1999).

Ramachandran plots of ψ vs. ϕ for each residue of each TMD were generated, collecting data points every 5 ps over the whole trajectory. Nearly all plots (not shown) simply show a well-defined single group of points proximate to mean values from Table 1. Notable exceptions are plots for dihedrals of residues 652 and 653 of each TMD (towards the N-terminal end), where the group of points is more diffuse, and in the case of residue 652 of the charged mutant TMD, where there is more than one distinct group of points. These exceptions reflect unwinding of the α helix at that end of the TMD. There is little unwinding of the α helix at the C-terminal end of each TMD, and this is reflected in the Ramachandran plots for the residues at that end. As discussed in the next section, there is π-helical hydrogen bonding ($i \rightarrow i+5$) present in the native and charged mutant TMD systems (between the oxygens of residues 672 and 673, and the hydrogens of 677 and 678, respectively). The $i \rightarrow i+5$ hydrogen bonding and resulting change of secondary structure there coincides with the anomalous Ramachandran plots for residues 675 and 676 of the native system and residue 675 of the charged mutant system, where data points significantly populate regions around $\psi = -70°$(the ideal backbone dihedral values for a π helix are $\phi = -57°$ and $\psi = -70°$).

Peptide backbone hydrogen-bonding stability

For the present purposes, a hydrogen bond was considered to exist when the O–H distance was less than 2.5 Å, and the N–H–O angle was greater than 135° (Kovacs et al. 1995). All such distances and angles were calculated from trajectories using CHARMM, sampling every 0.1 ps. The average and rms O_i–H_{i+4} distances (between the backbone oxygen atom O_i of the ith residue, and the backbone hydrogen atom H_{i+4} of residue $i+4$) for all three systems are shown in Fig. 2.

All three systems displayed average distances well within hydrogen bonding distance in the hydrophobic region and distal end (the very far end) of the C-terminal region of the peptide, but some were outside of hydrogen bonding distance at the N-terminal end. Some distances were also out of hydrogen bonding range at the C-terminal end just above the lipid headgroups for the charged mutant TMD (residues 672–675) and, to a lesser extent, for the native TMD (residues 673–675), but all distances in this region in the protonated mutant TMD were within hydrogen bonding range. Plots of the number of $i \rightarrow i+4$ hydrogen bonds as a function of time (Fig. 3) shed further light on this last observation. In the native system, the number of $i \rightarrow i+4$ hydrogen bonds initially dropped to about 20 on average (out of a possible 31) after a little over 1 ns of trajectory. Plots of individual O_i–H_{i+4} distances vs. time (not shown) show that oxygens O_{653}, O_{654}, O_{662}, O_{663}, O_{673}, O_{674}, and O_{675} were temporarily out of $i \rightarrow i+4$ hydrogen bonding distance at that point in time. These distances soon shrank back, restoring the number of $i \rightarrow i+4$ hydrogen bonds, but there was another drop in the number of hydrogen bonds further into the simulation (after about 7 ns of trajectory). That decrease involved the oxygens O_{672}, O_{673}, O_{674}, and O_{675} falling out of hydrogen bonding distance from their hydrogen mates four residues up, and those hydrogen bonds were not restored in the remaining length of trajectory. The same phenomenon was evident with the same oxygens in the charged mutant, but at a much earlier point in the trajectory (within the first nanosecond). The longer fraction of time spent out of $i \rightarrow i+4$ hydrogen bonding distance by those oxygens in the charged mutant system contributed to the greater average O_i–H_{i+4} distances seen in that system for those oxygens. In the case of the protonated mutant TMD, the number of $i \rightarrow i+4$ hydrogen bonds did not drop significantly at any point in the simulation.

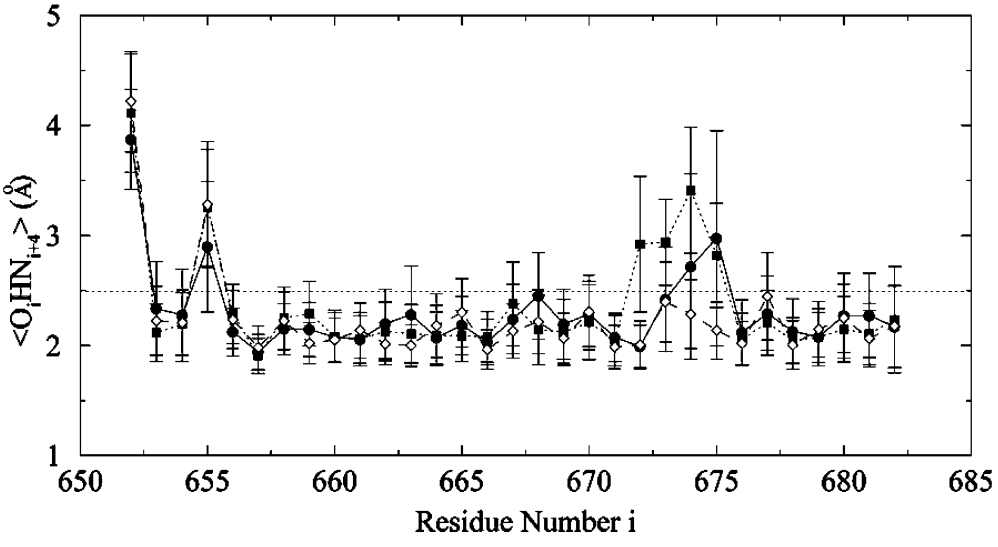

Fig. 2 Average and rms O_i–H_{i+4} distances for the native TMD (*filled circles and solid line*), charged mutant (*filled squares* and *dotted line*), and protonated mutant (*open diamonds* and *dashed line*). Residue numbering follows the amino acid sequence of Neu. The *dotted line* indicates the maximum distance allowable to count as a hydrogen bond (2.5 Å)

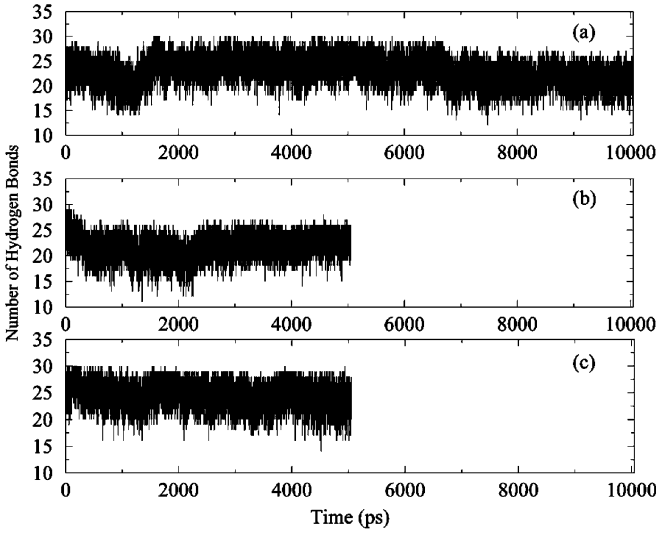

Fig. 3 The number of backbone $i \rightarrow i+4$ hydrogen bonds as a function of time for **a** the native TMD, **b** the charged mutant TMD, and **c** the protonated mutant TMD. The maximum number of inter-residue hydrogen bonds at any one time is 31

The breaking of $i \rightarrow i+4$ hydrogen bonds in the C-terminal region of the native and charged mutant TMDs just above the lipid headgroups coincided with the formation of $i \rightarrow i+5$ (π-helix) bonds there. Plots of individual O_i–H_{i+5} distances (not shown) show that O_{672} and O_{673} came into hydrogen bonding distance with hydrogen mates five residues up within the first nanosecond for the charged mutant TMD, and near $t = 7$ ns for the native TMD. In each case, they stayed within hydrogen bonding distance for the rest of their respective trajectories. Counts of the number of $i \rightarrow i+5$ hydrogen bonds throughout each TMD show that $i \rightarrow i+5$ hydrogen bonds (at most 2 at a given instant) appeared only during those respective time periods. The protonated mutant TMD displayed essentially no $i \rightarrow i+5$ hydrogen bonding throughout the length of the simulation. In all TMDs, there was no evidence of π-helix transitions within the hydrophobic region of the peptide, akin to what has been reported previously (Garnier et al. 1994, 2003; Duneau et al 1996, 1997, 1999; Sajot and Genest 2000). The $i \rightarrow i+5$ hydrogen bonds that did form appeared to replace the irreversibly broken (over the course of the trajectories) $i \rightarrow i+4$ hydrogen bonds in the C-terminal region of the native and charged mutant TMDs just above the lipid headgroups. This alteration of structure left a kink in the backbones of the native and charged mutant TMDs, which is illustrated in Fig. 4.

Note that the kinks were formed near Gly^{677} and that glycine tends to destabilize helices because of its considerable conformational freedom (O'Neil and DeGrado, 1990). More will be said on these observations in the Conclusions section.

Changes in the shape and tilt angle of the TMD: comparison by backbone principal moments of inertia

Plots of the principal moments of inertia of the backbone of each TMD versus time are shown in Fig. 5. I_{xx} and I_{yy} decreased simultaneously within the first nanosecond of trajectory for the charged mutant TMD, and near $t = 7$ ns for the native TMD. The magnitude of the decrease in each case was roughly the same, and there was no further significant change in these quantities in

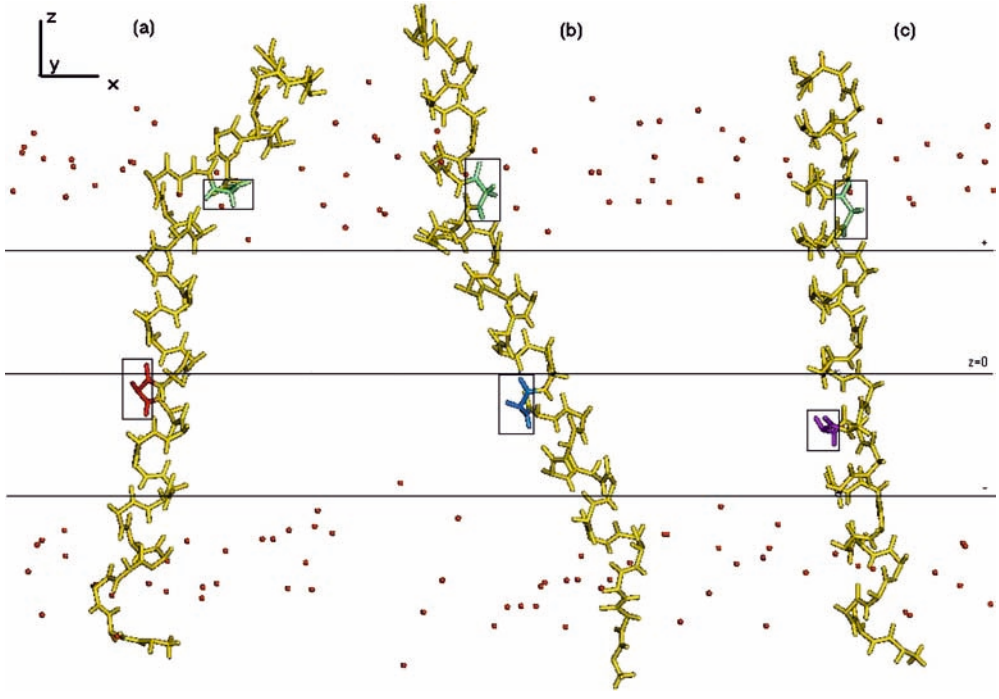

Fig. 4 The TMD backbones for **a** the native system, **b** the charged mutant system, and **c** the protonated mutant system, as they are at the end of their respective trajectories. The Val^{664} residue in **a** is shown in *red*, the charged Glu^{664} residue in **b** is shown in *blue*, and the protonated Glu^{664} residue in **c** is shown in *violet*. The Gly^{677} residue in each of the TMDs is shown in *pale green*. All of these residues are displayed with *boxes* around them. The *orange-red atoms* are nitrogen and oxygen atoms from the lipid headgroups, forming boundary markers for the lipid bilayer. The y axis is directed into the page. *Lines* for $z = 0$ and ± 10 Å have been drawn in for reference. The N terminus of each TMD lies below $z = 0$, and the C terminus of each TMD lies above $z = 0$

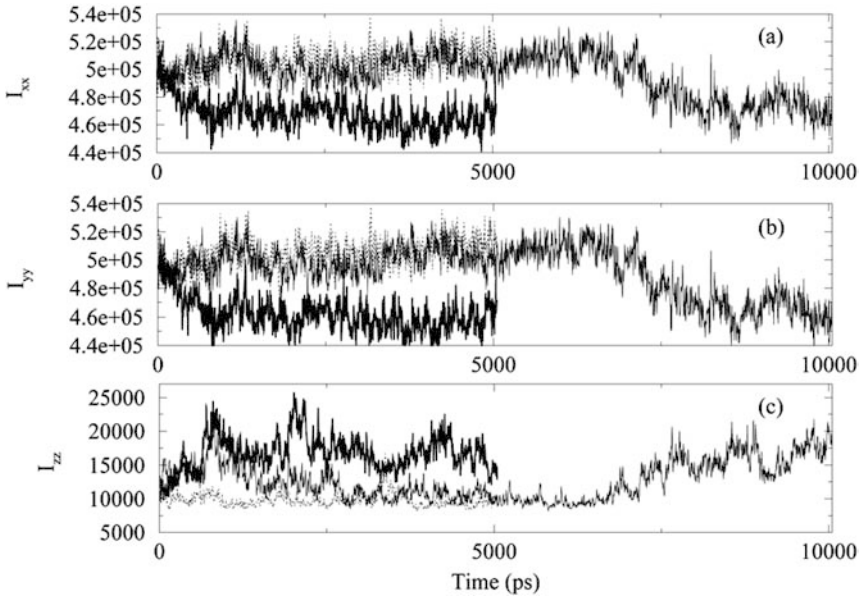

Fig. 5 Principal moments of inertia of the peptides in the **a** x-, **b** y-, and **c** z-directions, sampling every 5 ps. The *thin solid lines* are for the native TMD, the *thicker solid lines* are for the charged mutant TMD, and the *dotted lines* are for the protonated mutant TMD. Units are in (a.u. Å^2)

the remainder of their respective trajectories. Concomitant with decreases in I_{xx} and I_{yy}, the principal component I_{zz} increased. These changes reflect the kink formation in the TMD backbone above the lipid headgroups at the C-terminal end discussed in the previous section. The principal moments of inertia of the protonated mutant TMD backbone, which retained its α-helical structure and showed no deformation in structure throughout the simulation, showed no significant changes over the span of trajectory simulated.

A rotation matrix can be formed from the eigenvectors for the principal axes associated with the principal moments of inertia. From this matrix, Euler angles α, β, and γ, describing the orientation of these principal axes can be extracted. The angle β measures the angle between the z principal axis and the z-axis of the simulation coordinate system (along the bilayer normal), and therefore directly measures the tilting of the peptide helix axis from the bilayer normal. Figure 6 shows this angle as a function of time for each of the three TMDs. Each TMD began its simulation with zero degrees of tilt with respect to the z-axis. Note that over the course of the trajectories, the native TMD tilts by up to 20°, the charged mutant TMD tilts about the same amount, up to slightly more than 20°, and the protonated mutant TMD tilts even more, up to 25–30°. This is to be compared with the tilt angles measured by Smith et al. (1996) using polarized FTIR spectroscopy. By their measurements, in DMPC, native Neu is tilted by 20–25°, and mutant Neu (argued to be charged at Glu^{664} in DMPC) by 30–35°. When DMPS (negatively charged in the headgroup) is added to the bilayer, Glu^{664} is argued to be protonated, and the tilting reduces to angles comparable to native Neu. A more recent measurement shows that mutant Neu tilts by about 20° in POPC:POPS lipid bilayers (Smith et al. 2002). What is evident from the simulations presented here is that both mutants tilt more than the native TMD, and although the TMD

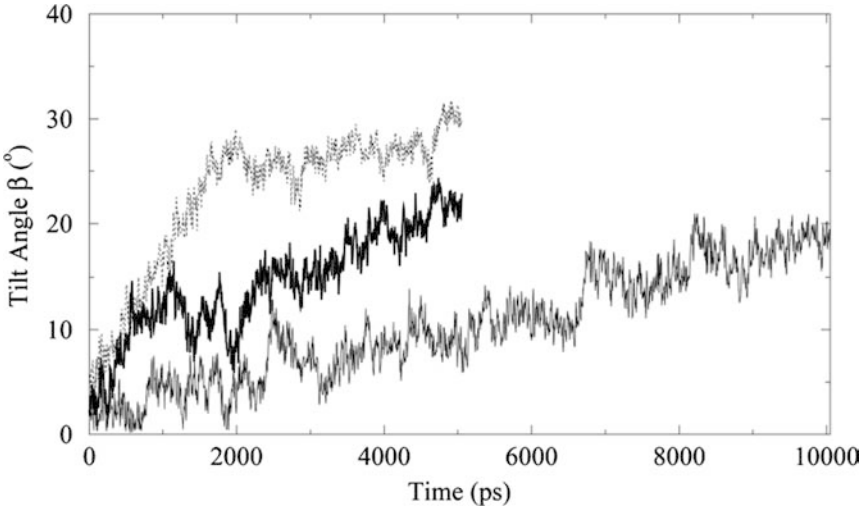

Fig. 6 The Euler angle β measuring tilt of the peptide helix axis from the bilayer normal is plotted against time for the native (*thin solid line*), charged mutant (*thicker solid line*), and protonated mutant (*dotted line*) systems

tilt angle may not have reached its equilibrium value by the end of the simulation trajectories, the mutant peptides both tilt earlier in the trajectory than the native peptide, and the protonated mutant TMD tilts earliest and the most of all three TMDs.

TMD center of mass

The centre of mass $\mathbf{R}_C$ of the backbone of each peptide was calculated from

$$\mathbf{R}_c = \frac{1}{M}\sum_{k=1}^{N} m_k \mathbf{r}_k, \tag{4}$$

where M is the total mass of the N backbone atoms, the kth one having mass m_k and position $\boldsymbol{r}_k$. In all cases, the x and y coordinates were constrained about the origin by a potential $V = k(x^2 + y^2)$, where k is 5 kcal/mol. Using $V = RT$ (applying the equipartition theorem), the root mean square fluctuation in each of the x and y dimensions calculates to be 0.35 Å, which agrees with the size of the fluctuations seen.

However, the z coordinate of the TMD center of mass was free to drift as it pleased during the simulation. In the case of the charged mutant TMD, the z coordinate fluctuated between $z = +2$ and $+4$ Å, and that of the protonated mutant fluctuated between $z = 0$ and $+3$ Å. In the case of the native TMD, it spent much of its time between $+3.5$ and $+6$ Å (see Fig. 7). Thus, the hydrophobic matching sought when positioning each TMD along the z-axis prior to surrounding it with DMPC lipids appears to have been sufficient to keep the peptide in place in the membrane. That the average z coordinate of the center of mass of the native TMD is consistently more positive than for the other TMDs correlates with the fact that the C-terminal end of the native TMD is more extended in the z direction than the other TMDs, due at least in part to its smaller tilt relative to the bilayer normal. Similarly, the z coordinate of residue 664's C_α atom for the native and mutant TMDs follow the same pattern. The C_α of residue 664 of the native TMD sits closer to the centre of the bilayer than that of either of the mutant TMDs. This may be due to the necessity to hydrate the polar Glu^{664} side chain (see below).

Solvation at the mutation site

Figure 8 shows the radial distribution functions of water molecules about each of the oxygens of Glu^{664} for the charged and protonated mutant systems. Both cases show a sharp peak at 2.7 Å, indicating a well-defined first shell of hydration. The maximum value for the protonated case (Fig. 8b) is a factor of 5 less than that for the charged case (Fig. 8a), indicating that water molecules are five times less likely to be found at that location in the protonated case than in the charged case. It is also significantly less than 1 (meaning that water molecules are less likely to be found there than at a corresponding distance in bulk water). CHARMM does not allow the hydrogen atom to be shared between the carboxylic oxygens of glutamic acid, associating the protonating hydrogen atom with only one of the two oxygen atoms. Consequently, the radial distribution function of the two oxygen atoms are different from each other when Glu^{664} is protonated. The distribution function for oxygen OE2 (assumed protonated) possesses a better-defined second shell of hydration, at about 4.4 Å, and a slightly smaller probability of hydration in the first shell, when compared to that for oxygen OE1 (unprotonated).

Cross-multiplying Eq. (2) by $\rho_i \Delta V(r_{ij})$ and integrating over r_{ij} gives the number of waters of solvation. In the case of the charged mutant TMD, integrating over the first hydration peak (from $r_{ij} = 2.5$ Å to $r_{ij} = 3.4$ Å) results in a total of three water molecules for each of the Glu^{664} carboxyl oxygens. For the protonated Glu^{664} case, this results in a total of 0.54 water molecules for the protonated OE2 oxygen, and one water molecule for the unprotonated OE1 oxygen. The protonated OE2 oxygen shows a well-defined second shell of hydration, and integrating under that shell (from $r_{ij} = 3.4$ Å to $r_{ij} = 5.7$ Å) gives approximately another 5.5 water molecules. These estimates are affected by the ambiguity in

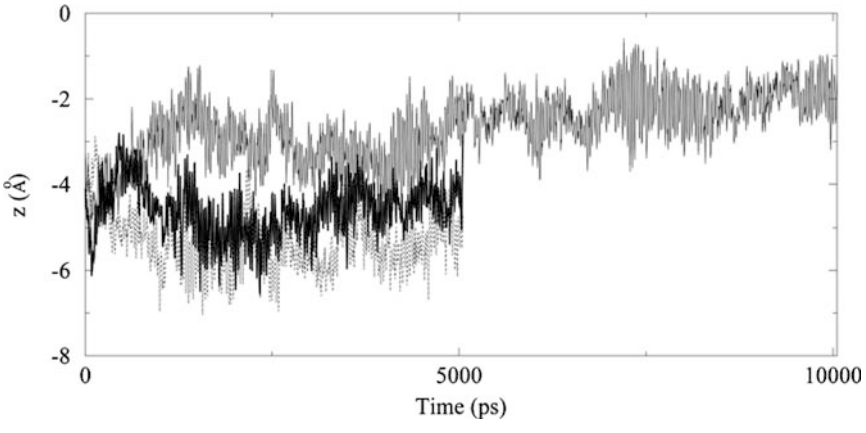

Fig. 7 The z coordinate of the C_α atom of amino acid residue 664 as a function of time for the native (*thin solid line*), charged mutant (*thicker solid line*), and protonated mutant (*dotted line*) TMDs

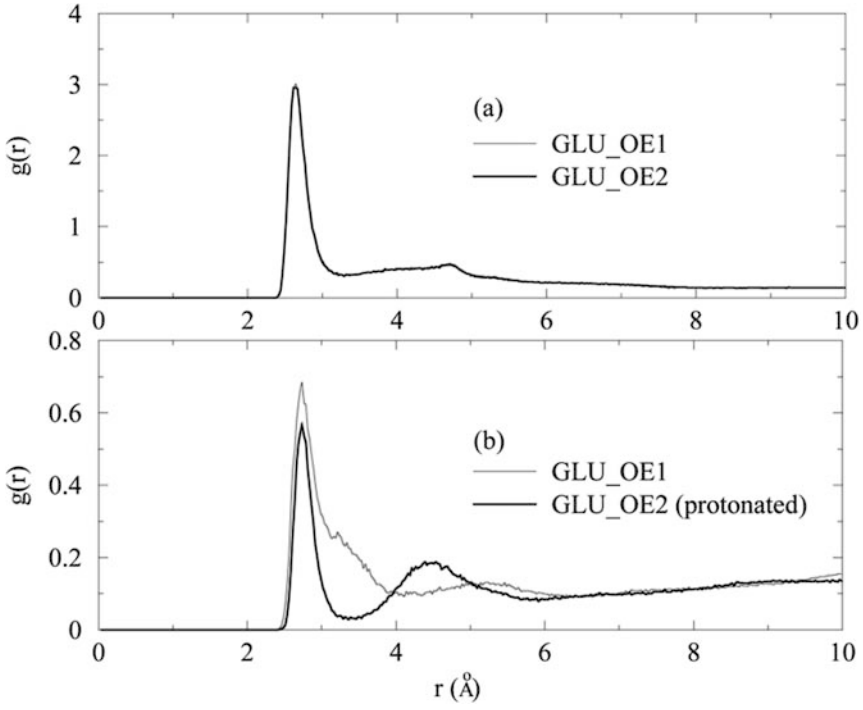

Fig. 8 Radial distribution functions about each of the side-chain carboxyl oxygens of Glu^{664}. In the case of the charged mutant system (**a**), both oxygens are unprotonated. In the case of the protonated mutant (**b**), oxygen OE1 is unprotonated, and oxygen OE2 is protonated

deciding where to start and (particularly) where to stop integrating. The integration under the first shell of hydration, for example, could arguably be stopped between 3.2 and 3.6 Å. This introduces an uncertainty of about 10% in the case of the charged mutant TMD, and for the protonated mutant TMD, a 4% uncertainty for the protonated oxygen atom and 20% uncertainty for the unprotonated oxygen atom. The second shell of hydration for the protonated oxygen atom has an uncertainty of 5% in the integration result.

The space-filling models shown in Fig. 9 compare the number of water molecules that are attracted to the carboxyl oxygens of Glu^{664} for the charged and protonated mutant TMDs. The water molecules appear to find their way around lipid molecules to the oxygen atoms of Glu^{664}, helped by the fact that the TMD tilts these oxygen atoms towards the water molecules at the nearest lipid headgroup–water interface. The water penetration appears not have any tendency to "squash" the lipid bilayer leaflet. We have measured the lipid bilayer thickness as a function of trajectory time and find bilayers in the charged mutant and protonated mutant TMD systems to be actually thicker (at about 34 Å) than the bilayer in the native TMD system (at 32–33 Å), wherein there is no substantial water penetration of this kind to be seen. We also ran a control DMPC bilayer simulation (consisting of 36 lipids, 18 in each leaflet, constructed in the same fashion as the TMD systems),

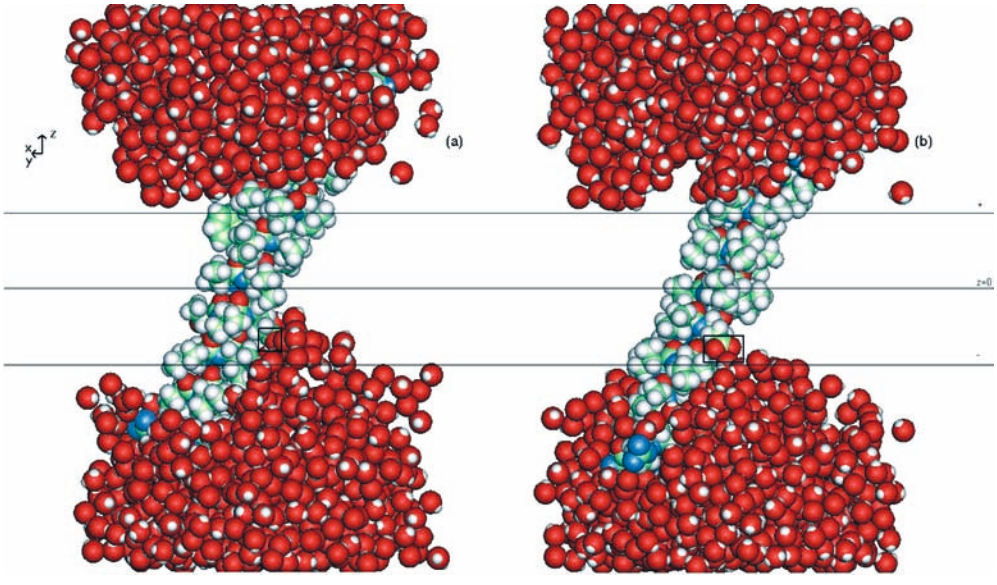

Fig. 9 Solvation of Glu^{664} in the **a** charged mutant and **b** protonated mutant TMDs, shown at t = 5.05 ns. A *box* is drawn around the oxygens of Glu^{664} where they are visible in each picture. In each picture, the *y*-axis of the coordinate system points obliquely out of the page, and the *x*-axis points obliquely into the page (each at 45°). *Lines* for z = 0, ±10 Å have been drawn in for reference. Lipid molecules have been omitted for clarity

which gave the same bilayer thickness as for the mutant TMD systems, over the same trajectory time (data not shown).

The large pocket of water molecules that penetrates into the hydrocarbon region of the membrane lipid molecules is remarkable, especially in the case of the charged mutant TMD. The observation of water penetration into the hydrophobic domain of lipid bilayers is nothing new. This has been seen in MD simulations of membrane-bound protein channels, such as Influenza A M2 (Forrest et al. 2000) and Alamethicin (Tieleman et al. 1999), as well as in a simulation of the lytic behaviour of melittin (Bernèche et al. 1998). Further, it has been shown experimentally that water molecules penetrate the core of membranes more readily in the presence of membrane-bound proteins (Ho and Stubbs 1992) or small peptides (Jacobs and White 1989).

However, if the energy cost of water penetration into the hydrophobic region of the membrane, in the case of mutated Neu TMDs, and of drawing the TMD towards the water interface is significant, it may be energetically favourable for two $Val^{664} \rightarrow Glu$ mutant Neu TMDs to share a single water pocket. This process would not occur with the native sequence which has a hydrophobic residue (Val) at that position.

Thus, the occurrence of significant water penetration into the hydrophobic region of the lipid bilayer may be a contributing factor to the spontaneous dimerization of $Val^{664} \rightarrow Glu$ mutant Neu. Much is unknown about the actual mechanism of the dimerization and activation of $Val^{664} \rightarrow Glu$ mutant Neu; however, it is widely felt that highly specific side-chain interactions are involved. For example, replacing Val^{664} with Gly, His, Lys, or Tyr does not activate the Neu receptor, but substituting with Glu^{664}, Gln^{664}, or (to a lesser extent) Asp^{664} does activate the Neu receptor (Bargmann and Weinberg 1988). Significantly, the side chains of Glu and Gln are derivatives of one another, while the side chain of Asp, though similar to Glu, is shorter by one methylene group. The other side chains are significantly different in their structure and chemical properties. It has also been shown that dimerization is not sufficient for cellular transformation, as it is possible to generate mutants of Neu that spontaneously dimerize but do not spontaneously activate the receptor (Cao et al. 1992b). There has been some recent progress in attempting to determine the residues that are essential for receptor dimerization and activation, but more work lies ahead in this area (Burke and Stern 1998; Sajot and Genest 2000). Even less is known about the dimerization process for native Neu.

Conclusions

As explained in the introduction, detailed physical characterization of the TMD of a rat integral membrane protein, Neu, in its native and mutant forms, could lead to a better understanding of the role that it plays in normal and aberrant signal transduction processes. To this end, results of comparative molecular dynamics simulations of native and (both protonated and unprotonated) mutant Neu transmembrane segments in fully hydrated DMPC bilayers have been presented in this paper. As we have shown in this work, subtle differences between the three systems are apparent which relate to past observations seen via both experimental and computer modelling approaches.

Smith et al. (1996) suggested, based on their data, that the α-helical conformation of the charged mutant TMD in the presence of DMPC should unravel at the N-terminal end to expose the charged carboxyl group of Glu^{664} to lipid polar headgroups. Later work by Smith et al. (2002), however, demonstrated that residues 662 to 665 (lying between the lipid headgroups and the mutation site, position 664) are also in an α-helical conformation in the mutant Neu TMD. Our work supports the latter notion. Analysis of TMD backbone dihedral angles, ϕ and ψ, over time through Ramachandran plots, and of their average and rms values, shows that the α-helical structure of each of these TMDs (including the unprotonated mutant) is generally very stable. TMD backbone hydrogen bonding shows a preponderance of $i \rightarrow i+4$ hydrogen bonding (indicative of the α-helical conformation) throughout much of each TMD helix for the extent of the simulation trajectory. Kinking of secondary structure at the C-terminal end just above the lipid headgroups, in the case of the native and charged mutant TMD systems, introduces stable $i \rightarrow i+5$ hydrogen bonding, which is otherwise absent in all three TMDs. The presence of the kinking in TMD secondary structure is confirmed in the time evolution of the sizes of the principal moments of inertia of the TMD backbones. The formation of π-helix bulges, reported in detail by Duneau et al. (1996, 1999) and Garnier and co-workers (2003) in their molecular dynamics simulations of c-ErbB2, particularly around the mutation site in the mutant TMDs, is absent in the present simulations. Formation of π bulges can be frequent features of the structural dynamics of flexible α helices. When a π bulge forms, residues are redistributed over the face of the helix. π bulges could induce important modifications in the interface between interacting helices to bring about dimerization. There has been experimental evidence cited for π-bulge transitions in the TMD secondary structure of Neu (Goetz et al. 2001), but Houliston et al. (2003) have not observed them. What is notable, however, is that the π bulge reported by Goetz et al. occurs towards the C-terminus end of the TM-spanning segment, near the position where we observe kinking in the native and charged mutant TMD simulations. On the other hand, it is worthwhile to note a recent study by Feig et al. (2003) which suggests that virtually all common MD force fields, including the ones used in this study and in that of Duneau et al., tend to overestimate how favorable π-helix formation is.

Smith et al. (1996) also showed that the wild-type Neu TMD in DMPC tilts with respect to the bilayer normal by 20–25°, and that the mutant Neu TMD in the same environment tilts by 30–35°. They further showed

that incorporating DMPS—which, they argued, shifts the pK_a of Glu^{664} so that this residue becomes protonated—decreases the tilt to an angle comparable to that exhibited by the native TMD. Our results are in partial agreement on this point; the native TMD tilts up to 20° by the end of the simulation, but, in contrast, the protonated mutant TMD tilts about 30–35° and the unprotonated mutant TMD tilts 20–25°. However, it is to be noted in this comparison, the TMDs, particularly the native and charged mutant types, appear not to have achieved an equilibrium tilt angle in the trajectory time of the simulations (see Fig. 6).

At this point, it is worth considering whether the small system size would have any effect in this tilting. The small lipid bilayer may tilt its chains in concert with the TMD, encouraging the TMD tilt. We have measured the average tilt of the lipid z principal axis (of the moment of inertia tensor for each lipid) from the bilayer normal, as well as the average lipid-chain tilt (measured as the angle between the bilayer normal and the average vector connecting the C2–C3 bond, near the glycerol and headgroup, and the C6–C7 bond, further down in the chain, averaging over both *sn*-1 and *sn*-2 chains), in each system (data not shown). These results are also compared to those for a pure DMPC lipid bilayer system that we simulated at the same time. The average tilt of the lipid z principal axis was considerably greater for both mutant TMD systems (30–35°), than for both the native TMD system and pure lipid system (each 20–25°). Similar results are seen in the average lipid chain tilt (20–30° for the mutant TMD system lipids, and 5–10° for the pure lipid and native TMD system lipids). Note the lower degree of lipid tilt in the native TMD system, comparable to that of our pure lipid bilayer system in both instances, in spite of the considerable TMD tilt that is seen in the native system. This suggests that the TMD tilt witnessed, particularly in the native TMD system, is not correlated with lipid tilt, in spite of the small system size. As to why the mutant TMD systems have greater average lipid tilt, one can only speculate. Garnier et al. (2003) have noticed in their simulation of ErbB2 dimer in a DMPC bilayer that lipids tend to be more disordered closer to the dimer than those that are further away. The solvation of Glu^{664}, involving both water penetration and tilting of the Glu^{664} towards the water molecules, may play a role in our greater lipid tilt.

What is remarkable about the results of the simulations we have performed is the presence of water molecules that penetrate into the hydrophobic region of the lipid bilayer to hydrate the carboxyl group of the Glu^{664} residue in the case of the mutant TMDs (absent in the case of the native TMD). The suggestion of Smith et al. (1996) that the α helix of the unprotonated mutant TMD should unravel so that the carboxyl group of Glu^{664} is exposed to lipid headgroups is apparently less favorable than water molecules entering the hydrophobic region of the lipid bilayer to hydrate this group. We even see this water penetration occuring, although to a lesser extent, in the case of the protonated mutant TMD. Studies of native and mutant TMDs in detergent micelles (in ^2H buffer) by solution state ^1H NMR reveal that the amide hydrogens near the mutation site of the mutant sequence exchange rapidly, whereas the corresponding amides of the native TMD exchange extremely slowly (Houliston, et al. 2004), suggesting enhanced solvent accessibility near the mutation site.

The presence of hydrating water in the hydrophobic region of the lipid bilayer in the cases of the mutant TMDs and its absence in the case of the native TMD is correlated with the center of mass of the mutant TMDs sitting higher in the membrane (closer to a membrane edge) than the native TMD. In this way, the C_α atom of residue 664 is brought closer to polar lipid headgroups and hydrating water molecules in the mutant case than in the native case. It is notable that the center of mass of the unprotonated mutant TMD is higher than the center of mass of the protonated mutant TMD throughout their simulation trajectories (Fig. 7). It is likely for this reason that we see the protonated mutant TMD tilting more than the unprotonated TMD in our simulations, so that the carboxyl group of Glu^{664} is brought close to hydrating water molecules in each case (see Figs. 4 and 9). In other words, hydration of Glu^{664} is likely a significant factor in determining the degree of tilt of each type of TMD.

What could encourage hydration of Glu^{664} even further is if a second mutant TMD was close by, such that the carboxyl group of its Glu^{664} residue and its water molecules of hydration came into "close contact" with that of the first TMD. The hydrophobic effect would draw the two TMDs closer together to share their hydrating water molecules, so that fewer water molecules need be present in the hydrophobic region of the lipid bilayer to keep the two carboxyl groups sufficiently hydrated. Indeed, Garnier et al. (2003) witness the formation of water bridges between opposing Glu^{664} residues in a ErbB2 dimer they simulated in a hydrated DMPC bilayer. Therefore, the presence of hydrating water molecules in the hydrophobic region of the lipid bilayer and the drive of the hydrophobic effect could help stimulate the spontaneous dimerization of $Val^{664} \rightarrow Glu$ mutant Neu. As we have argued in the Results and Discussion section of this paper, little is known about the mechanism for dimerization and activation of $Val^{664} \rightarrow Glu$ mutant Neu and even less for native Neu.

Some words should be said about some of the limitations of these simulations. As has been pointed out earlier in this paper, it has become increasingly common to employ Ewald summation techniques in MD simulations to avoid the use of cutoffs in calculating electrostatic interactions (Patra et al. 2003). Some systematic studies have recently been carried out (Anézo et al. 2003; Patra et al. 2003) that compare cutoff techniques with PME techniques in MD simulations of dipalmitoylphosphatidylcholine (DPPC) bilayers, and several artifacts from cutoff-based calculations were evident. These are primarily seen in the lateral dipole moment of the bilayer and in the ordering of lipid chains, lipid

headgroups, and water molecules in the vicinity of the lipid–water interface. Some of these effects are mitigated by employing switching functions to smooth the cutoff transition (Anézo et al. 2003), which we have used in each of our simulations. Another obvious limitation is the length of trajectory. As pointed out by Anézo et al. (2003), trajectories of 5–10 ns are often not sufficiently long to reach equilibrium conditions in lipid bilayer systems: lengths of up to 25 ns are sometimes needed. That our systems may not have reached equilibrium is evident, for example, in the slow tilt of the TMDs with respect to the bilayer normal (see Fig. 6).

We believe that these comparative molecular dynamics simulations of native and (both protonated and unprotonated) mutant Neu transmembrane segments have shed some light on their physical behaviour. While some of the subtle differences noted in this study may simply reflect the variability expected even for isolated "video-clips" (5–10 ns in duration) of identical systems, other features, most notably the greater helix tilt and the higher hydration level of the mutant TMD, are likely the direct result of the inclusion of a hydrophilic residue within the transbilayer region. Clearly, however, a considerable amount of further work is needed—through both experiment and computer modelling—to come to a better and more detailed understanding of the physical processes that result from the $Va^{l664} \rightarrow Glu$ point mutation in the transmembrane domain of Neu.

Acknowledgements We would like to thank Professor Bernie Nickel of the Department of Physics at the University of Guelph and Simon Bernèche and Professor Benoit Roux of the Departments of Chemistry and Physics at the Université de Montréal. This work was supported by grants from the Natural Sciences and Engineering Research Council of Canada (NSERC). B.M.V. was supported by a NSERC PGS A scholarship in the course of this work.

References

Anézo C, de Vries AH, Höltje H-D, Tieleman DP, Marrink S-J (2003) Methodological issues in lipid bilayer simulations. J Phys Chem 107:9424–9433

Bargmann CI, Weinberg RA (1988) Oncogenic activation of the *neu*-encoded receptor protein by point mutation and deletion. EMBO J 7:2043–2052

Bargmann CI, Hung MC, Weinberg RA (1986a) Multiple independent activations of the *neu* oncogene by a point mutation altering the transmembrane domain of p185. Cell 45:649–657

Bargmann CI, Hung MC, Weinberg RA (1986b) The *neu* oncogene encodes an epidermal growth factor receptor-related protein. Nature 319:226–230

Belohorcová K, Davis JH, Woolf TB, Roux B (1997) Structure and dynamics of an amphiphilic peptide in a lipid bilayer: a molecular dynamics study. Biophys J 73:3039–3055

Bernèche S, Roux B (2000) Molecular dynamics of the KcsA K^+ channel in a bilayer membrane. Biophys J 78:2900–2917

Bernèche S, Nina M, Roux B (1998) Molecular dynamics simulation of melittin in a dimyristoylphosphatidylcholine bilayer membrane. Biophys J 75:1603–1618

Brandt-Rauf PW, Pincus MR, Monaco R (1995) Conformation of the transmembrane domain of the c-erbB-2 oncogene-encoded protein in its monomeric and dimeric states. J Protein Chem 14:33–40

Brennan PJ, Kumogai T, Berezov A, Murali R, Greene MI (2000) HER2/Neu: mechanisms of dimerization/oligomerization. Oncogene 19:6093–6101

Brooks BR, Bruccoleri RE, Olafson BD, States DJ, Swaminathan S, Karplus M (1983) CHARMM: a program for macromolecular energy, minimization, and dynamics calculations. J Comp Chem 4:187–217

Burke C, Stern DF (1998) Activation of Neu (ErbB-2) mediated by disulfide bond-induced dimerization reveals a receptor tyrosine kinase dimer interface. Mol Cell Biol 18:5371–5379

Cao H, Bangalore L, Bormann BJ, Stern DF (1992a) A subdomain in the transmembrane domain is necessary for $p185^{neu*}$ activation. EMBO J 11:923–932

Cao H, Bangalore L, Dompe C, Bormann BJ, Stern DF (1992b) An extra cysteine proximal to the transmembrane domain induces crosslinking of $p185^{neu}$ and $p185^{neu*}$. J Biol Chem 267:20489–20492

Cho H-S, Mason K, Ramyar KX, Stanley AM, Gabelli SB, Denney Jr. DW, and Leahy DJ. (2003) Structure of the extracellular region of Her2 alone and in complex with the herceptin Fab. Nature 421:756–760

Creighton TE (1984) Proteins: structures and molecular properties. WH Freeman, New York

Darden T, York D, Pederson L (1993) Particle mesh Ewald: an n·log(n) method for Ewald sums in large systems. J Chem Phys 98:10089–10092.

Davis J H, Auger M (1999) Static and magic angle spinning NMR of membrane peptides and proteins. Prog NMR Spectrosc 35:1–84

De Loof H, Harvey SC, Segrest JP, Pastor RW (1991) Mean field stochastic boundary molecular dynamics simulation of a phospholipid in a membrane. Biochemistry 30:2099–2113

Dunbrack RL, Karplus M (1993) Backbone-dependent rotamer library for proteins. J Mol Biol 230:543–574

Duneau J-P, Genest D, Genest M (1996) Detailed description of an α-helix $\rightarrow$ π-bulge transition detected by molecular dynamics simulations of the $p185^{c\text{-}erbB2}$ V659G transmembrane domain. J Biomol Struct Dyn 13:753–769

Duneau J-P, Garnier N, Genest M (1997) Insight into signal transduction: structural alterations in transmembrane helices probed by multi- 1 ns molecular dynamics simulations. J Biomol Struct Dyn 15:555–572

Duneau J-P, Crouzy S, Garnier N, Chapron Y, Genest M (1999) Molecular dynamics simulations of the *erbB-2* transmembrane domain within an explicit membrane environment: comparison with vacuum simulations. Biophys Chem 76:35–53

Egberts E, Marrink SJ, Berendsen HJC (1994) Molecular dynamics simulation of a phospholipid membrane. Eur Biophys J 22:423–436

Engh RA, Huber R (1991) Accurate bond and angle parameters for x-ray protein structure refinement. Acta Cryst A47:392–400

Feig M, MacKerell AD Jr, Brooks CL III (2003) Force field influence on the observation of π-helical protein structures in molecular dynamics simulations. J Phys Chem B 107:2831–2836

Feller SE, Zhang Y, Pastor RW, Brooks BR (1995) Constant pressure molecular dynamics simulation: the Langevin piston method. J Chem Phys 103:4613–4621

Finean JB, Coleman R, Michell RH (1984) Membranes and their cellular functions, 3rd edn. Blackwell, Boston

Fleishman FJ, Schlessinger J, Ben-Tal N (2003) A putative molecular-activation switch in the transmembrane domain of erbB2. Proc Natl Acad Sci USA 99:15937–15940

Forrest LR, Kukol A, Arkin IT, Tieleman DP, Sansom MSP (2000) Exploring models of the influenza A M2 channel: MD simulations in a phospholipid bilayer. Biophys J 78:55–69

Franks NP (1976) Structural analysis of hydrated egg lecithin and cholesterol bilayers I. X-ray diffraction. J Mol Biol 100:345–358

Garnier N, Genest D, Duneau J-P, Genest M (1994) Influence of a mutation in the transmembrane domain of the $p185^{c\text{-}erbB2}$ oncogene-encoded protein studied by molecular dynamics simulations. J Biomol Struct Dyn 11:983–1002

Garnier N, Genest D, Duneau J-P, Genest M (1997) Molecular modeling of c-*erbB2* receptor dimerization: coiled-coil structure of wild and oncogenic transmembrane domains—stabilization by interhelical hydrogen bonds in the oncogenic form. Biopolymers 42:157–168

Garnier N, Crouzy S, Genest M (2003) Molecular dynamics simulations of the transmembrane domain of the oncogenic ErbB2 receptor dimer in a DMPC bilayer. J Biomol Struct Dyn 21:179–199

Gennis R B (1989) Biomembranes: molecular structure and function. Springer, Berlin Heidelberg New York

Goetz M, Carlotti C, Bontemps F, Dufourc EJ (2001) Evidence for an α-helix $\rightarrow$ π-bulge helicity modulation for the Neu/ErbB-2 membrane-spanning segment. A ^{1}H NMR and circular dichroism study. Biochemistry 40:6534–6540

Goldstein DJ, Andresson T, Sparkowski JJ, Schlegel R (1992) The BPV-1 E5 protein, the 16 kDa membrane pore-forming protein and the PDGF receptor exist in a complex that is dependent on hydrophobic transmembrane interactions. EMBO J 11:4851–4859

Gullick WJ, Bottomley AC, Lofts FJ, Doak DG, Mulvey D, Newman R, Crumpton JJ, Sternberg MJ, Campbell ID (1992) Three dimensional structure of the transmembrane region of the proto-oncogenic and oncogenic forms of the Neu protein. EMBO J 11:43–48

Haile JM (1992) Molecular dynamics simulations: elementary methods. John Wiley, Toronto

Hardy BJ, Pastor RW (1994) Conformational sampling of hydrocarbon lipid chains in an orienting potential. J Comp Chem 15:208–226

Ho C, Stubbs CD (1992) Hydration at the membrane protein–lipid interface. Biophys J 63:897–902

Houliston RS, Hodges RS, Sharom FJ, Davis JH (2003) Comparison of proto-oncogenic and mutant forms of the transmembrane region of the Neu receptor in TFE. FEBS Lett 535:39–43

Houliston RS, Hodges RS, Sharom FJ, Davis JH (2004) Characterization of the proto-oncogenic and mutant forms of the transmembrane region of Neu in micelles. J Biol Chem (in press.)

Hynes NE, Stern DF (1994) The biology of erbB-2/*neu*/HER-2 and its role in cancer. Biochim Biophys Acta 1198:165–184.

Jacobs RE, White SH (1989) The nature of the hydrophobic binding of small peptides at the bilayer interface. Implications for the insertion of transbilayer helices. Biochemistry 28:3421–3437

Jorgensen WL, Chandrasekhar J, Madura JD, Impey RW, Klein ML (1983) Comparison of simple potential functions for simulating liquid water. J Chem Phys 79:926–935

Koenig BW, Strey HH, Gawrisch, K (1997) Membrane lateral compressibility determined by NMR and X-ray diffraction: effect of acyl chain polyunsaturation. Biophys J 73:1954–1966

Kovacs H, Mark AE, Johansson J, van Gunsteren WF (1995) The effect of environment on the stability of an integral membrane helix: molecular dynamics simulations of surfactant protein C in chloroform, methanol, and water. J Mol Biol 247:808–822

Mackerell AD, Bashford D, Bellot M, Dunbrack RL, Field MJ, Fischer S, Gao J, Guo H, Joseph D, Ha S, Kuchnir L, Kuczera K, Lau FTK, Matos C, Michnick S, Nguyen DT, Ngo T, Prodhom B, Roux B, Schlenkrich B, Smith J, Stote R, Staub J, Wiorkiewicz-Kuczera J, Karplus M (1992) Self-consistent parametrization of biomolecules for molecular modelling and condensed phase simulations. Biophys J 61:A143

Nelander JC, Blaurock AE (1978) Disorder in nerve myelin: phasing the higher order reflections by means of the diffuse scatter. J Mol Biol 118:497–532

Nosé S (1984a) Constant temperature molecular dynamics. J Chem Phys 81:511–519

Nosé S (1984b) A molecular dynamics method for simulations in the canonical ensemble. Mol Phys 52:255–268

O'Neil KT, DeGrado WF (1990) A thermodynamic scale for the helix-forming tendencies of the commonly occurring amino acids. Science 250:646–651

Pastor RW, Venable RM, Karplus M (1991) Model for the structure of the lipid bilayer. Proc Natl Acad Sci USA 88:892–896

Patra M, Karttunen M, Hyvönen MT, Falck E, Lindqvist P, Vattulainen I (2003) Molecular dynamics simulations of lipid bilayers: major artifacts due to truncating electrostatic interactions. Biophys J 84:3636–3645

Petrache HI, Tristam-Nagle S, Nagle JF (1998) Fluid phase structure of EPC and DMPC bilayers. Chem Phys Lipids 95:83–94

Petrache HI, Dodd SW, Brown MF (2000) Area per lipid and acyl length distributions in fluid phosphatidylcholines determined by ^{2}H NMR spectroscopy. Biophys J 79:3172–3192

Press MF, Bernstein L, Thomas PA, Meisner F, Zhou JY, Ma Y, Hung G, Robinson RA, Harris C, El-Naggar A, Slamon D J, Phillips RN, Ross JS, Wolman SR, Flom KJ (1997) HER-2 *neu* gene amplification characterized by fluorescence *in situ* hybridization: poor prognosis in node-negative breast carcinomas. J Clin Oncol 15:2894–2904

Roux B, Woolf TB (1996) Molecular dynamics of Pf1 coat protein in a phospholipid bilayer. In: Merz Jr KM, Roux B (eds) Biological membranes: a molecular perspective from computation and experiment. Birkhauser, Boston, pp 555–587

Ryckaert JP, Ciccotti G, Berendsen HJC (1977) Numerical integration of the Cartesian equations of motion of a system with constraints: molecular dynamics of n-alkanes. J Comp Phys 23:327–341

Sajot N, Genest M (2000) Structure prediction of the dimeric Neu/ErbB-2 transmembrane domain from multi-nanosecond molecular dynamics simulations. Eur Biophys J 28:648–662

Smith SO, Smith CS, Bormann BJ (1996) Strong hydrogen bonding interactions involving a buried glutamic acid in the transmembrane sequence of the Neu/ErbB-2 receptor. Nat Struct Biol 3:252–258

Smith SO, Smith C, Shekar S, Peersen O, Ziliox M, Aimoto S (2002) Transmembrane interactions in the activation of the Neu receptor tyrosine kinase. Biochemistry 41:9321–9332

Tieleman DP, Berendsen HJC, Sansom MSP (1999) An Alamethicin channel in a lipid bilayer: molecular dynamics simulations. Biophys J 76:1757–1769

Sternberg MJE, Gullick WJ (1990) A sequence motif in the transmembrane region of growth factor receptors with tyrosine kinase activity mediates dimerization. Prot Eng 3:245–248

Venable RM, Zhang Y, Hardy BJ, Pastor RW (1993) Molecular dynamics simulations of a lipid bilayer and of hexadecane: an investigation of membrane fluidity. Science 262:223–226

Verlet L (1967) Computer 'experiments' on classical fluids. I. Thermodynamical properties of Lennard-Jones molecules. Phys Rev 159:98–103

Weiner DB, Liu J, Cohen JA, Williams WV, Greene MI (1989) A point mutation in the Neu oncogene mimics ligand induction of receptor aggregation. Nature 339:230–231

Zhou FX, Merianos HJ, Brunger AT, Engelman DM (2001) Polar residues drive association of polyleucine transmembrane helices. Proc Natl Acad Sci USA 98:2250–2255